



Mechanochemical preparation of nanocrystalline stannite/chatkalite composite: kinetics of synthesis and thermoelectric properties

Peter Baláž¹ · Michal Rajňák² · Lenka Kubíčková^{3,4} · Mária Bali Hudáková¹ · Nina Daneu⁵ · Petr Levinský³ · Karel Knížek³ · Jiří Hejtmánek³ · Jiří Navrátil³ · Tomáš Kmječ⁴ · Robert Džunda⁶ · Marcela Achimovičová¹ · Olga Šestinová¹ · Matej Baláž¹

Received: 20 July 2023 / Accepted: 14 January 2024
© The Author(s) 2024

Abstract

In this study we demonstrate the use of Cu, Fe, Sn and S elemental precursors to synthesize chatkalite/stannite nanocomposite by high-energy milling in both lab-scale and industrial-scale mills. The products were characterized by XRD, SEM, HRTEM, EDX, Mössbauer spectroscopy and magnetometry. For the determination of optimum milling conditions, the magnetization data of the synthesized samples were used as output values using a Taguchi experimental design. The formation of the product proceeds via a multistep process comprising binary sulphides (SnS and CuS) formation at the beginning and chatkalite $\text{Cu}_6\text{FeSn}_2\text{S}_8$ /stannite $\text{Cu}_2\text{FeSnS}_4$ composite as the end products. The TEM images show tightly packed nanosized crystallites with the sizes in the range of tens of nanometers. Mössbauer study unveiled that iron is present in 3+ state instead of 2+ expected for stoichiometric phases. This discrepancy was explained by the presence of a small number of vacancies on Sn sites. Based on the thermoelectric measurements of the hot-pressed pellets, the calculated figure of merit reached a value of $ZT = 0.27$ at 600 K. The aim of this study is to prepare a representative of a promising class of environmentally acceptable thermoelectric materials in an environmentally sound solvent-free manner and characterize them while studying the kinetics of the reaction via magnetometry and the possibility to scale-up the solid-state synthesis process.

Keywords Chatkalite $\text{Cu}_6\text{FeSn}_2\text{S}_8$ · Stannite $\text{Cu}_2\text{FeSnS}_4$ · Mechanochemical synthesis · Magnetization · Thermoelectric performance · Scale-up

Introduction

Energy and the environment are the most significant concerns in the twenty-first century. They possess a driving force for an intensive research of corresponding energy materials and environmental science. In this connection, multinary sulphides as prospective energy materials represent great candidates, as they are composed from environmentally acceptable elements like Cu, Fe, Sn, Sb and S which substitute the scarce and toxic elements such as In, Ga, Te, Se, Pb and Cd used until now [1–7]. The multinary sulphides have many applications in the energy sector as optical materials [8–10], absorbers for solar cells [11] and thermoelectric materials [2–4, 12–16].

To synthesize multinary sulphides, the non-equilibrium recipes hold promise. Among them, mechanochemistry realized via high-energy milling plays the crucial role [17–27]. Besides perfect homogenization resulting in the uniform mixing of reacting elements, the chemical reactions taking

✉ Matej Baláž
balazm@saske.sk

¹ Institute of Geotechnics, Slovak Academy of Sciences, 04001 Košice, Slovakia

² Institute of Experimental Physics, Slovak Academy of Sciences, 04001 Košice, Slovakia

³ FZU - Institute of Physics of Czech Academy of Sciences, 16200 Prague 6, Czech Republic

⁴ Faculty of Mathematics and Physics, Charles University, V Holešovičkách 2, 18000 Prague 8, Czech Republic

⁵ Jozef Stefan Institute, 1000 Ljubljana, Slovenia

⁶ Institute of Materials Research, Slovak Academy of Sciences, 04001 Košice, Slovakia

place in parallel are strongly facilitated [28, 29]. One peculiarity of mechanochemistry is its ability to produce nanoparticles with a well-crystallized core, whereas the sub-surface regions are disordered. Another advantage is a scalability of the synthesis performed under environmentally friendly conditions with no gas evolution, absence of harmful solvents, using laboratory temperatures, etc. [17].

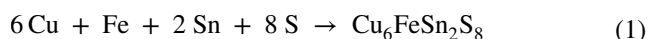
Several multinary sulphides have been prepared under these conditions, e.g. tetrahedrite [14], mohite [12, 30], mawsonite [31], stannite and rhodostannite [32–36], kessterite [11, 36] and colusite [10].

Chatkalite, $\text{Cu}_6\text{FeSn}_2\text{S}_8$ as a natural mineral was first discovered in Chatkal-Kuramin Mountains in Uzbekistan in 1981 [37, 38]. Later on, its occurrence was documented in Catamarca in Argentina [39]. It crystallizes in the tetragonal crystal system and its properties are close to stannite $\text{Cu}_2\text{FeSnS}_4$ and mawsonite $\text{Cu}_6\text{Fe}_2\text{SnS}_8$. Chatkalite belongs among the multinary semiconducting sulphides containing iron, which in its elemental form is strongly magnetic. However, its magnetization is reduced when Fe is being incorporated into semiconductor structure. Description of changes in magnetization data in systems where iron was used as solid state reactant in mechanochemical reactions was reported in previous studies [15, 27, 35, 40–43]. Several modes of application such as mechanochemical reduction and/or mechanochemical synthesis [21] using elemental iron were applied in the past.

It is the aim of this work to prepare and characterize a ternary sulphide belonging to the promising class of environmentally acceptable thermoelectric materials. The novelty which is governing this effort includes the application of magnetometry for the kinetic study of solid-state mechanochemical synthesis. The successful scale-up of this synthesis process represents a practical aspect of novelty, which is indispensable for future application.

Materials and methods

For mechanochemical synthesis of chatkalite $\text{Cu}_6\text{FeSn}_2\text{S}_8$ the following precursors were mixed in a stoichiometric ratio: copper (Merck, 99% purity), iron (Merck, 99% purity), tin (Nihon Seiko, 99% purity) and sulphur (CG-Chemikalien, 99% purity). The mixing of precursors for synthesis was realized according to the hypothetical equation



Two types of mills and the following milling conditions were used for mechanochemical synthesis:

- Laboratory planetary ball mill Pulverisette 7 premium line (Fritsch, Germany), batch mass 5–10 g. Precise

amount of sample was dependent on the experimental design of milling experiments according to Taguchi method. The milling was carried out in an argon atmosphere at revolutions of 400–800 min^{-1} using a tungsten carbide chamber (80 mL) filled with 135 g of balls (10 mm in diameter) from the same material. Milling was performed in duration 5–120 min. Each 30 minutes of milling were followed by 30 minutes break for cooling.

- Industrial eccentric vibratory ball mill ESM 656–0.5 ks (Siebtechnik, Germany), batch mass 100 g. The milling was carried out in an argon atmosphere at revolutions 960 min^{-1} using a satellite milling chamber from hardened steel (5 L) attached to the main corpus of the mill. The chamber was filled with 30 kg of tungsten carbide balls (35 mm in diameter). The amplitude of mill vibrations was 20 mm. Milling was performed for either 30 or 120 min. The principle of the mill operation in the industrial mill was described in our previous papers [14, 16].

XRD patterns of the milled samples were collected using a D8 Advance diffractometer (Bruker, Germany) with the (CuK_α radiation, Bragg–Brentano configuration). The generator was set up at 40 kV and 40 mA. The divergence and receiving slits were 0.3° and 0.1 mm, respectively. The XRD patterns were recorded in the range of $2\theta = 15 - 65^\circ$ with a step size 0.03°. For the phase identification the DiffracPlus Eva software and the ICDD PDF2 database was applied. The XRD patterns of the samples after hot pressing were collected using Bruker D8 Advance diffractometer (CuK_α , Lynxeye XE-T position sensitive detector) over the range of $2\theta = 15 - 60^\circ$ with a step size 0.02°. X-ray diffraction patterns were analyzed with the Rietveld method using the FULLPROF program [44]. The structures of detected phases were collected with the help of Inorganic Crystal Structure Database ICSD [45].

The magnetic measurements of the synthesized powders were performed by a vibrating sample magnetometer installed on a cryogen-free system equipped with 18 T superconducting magnet (Cryogenic Ltd., Great Britain). A magnetic moment of the vibrating samples was measured at a constant temperature of 298 K and in magnetic field ranging from 0 to 5 T. Subsequently, the magnetization values were calculated by dividing the magnetic moment values by the sample mass. For hot-pressed samples, the MPMS-XL magnetometer (Quantum Design, Inc., USA) was used. Degree of conversion α was calculated using equation

$$\alpha = (1 - M/M_{\text{max}}) \times 100 \quad (2)$$

where α is in %, M_{max} is the maximum saturation magnetization of the mixture of the non-reacting precursors and M is the saturation magnetization (both in $\text{A m}^2 \text{kg}^{-1}$) of the

synthesized samples. Both values of M and M_{\max} were taken at magnetic field 5 T.

The size and morphology of the powders were investigated with a scanning electron microscope (SEM) Tescan Vega 3 LMU (Tescan, Czechia) using accelerating voltage 20 kV. To secure electron conductivity the powders were covered by a layer of Au on fine coat ion sputter JFC 1100. To obtain elemental composition of powders, the energy dispersive X-ray (EDX) spectrometer Tescan: Bruker XFlash Detector 410 M (Bruker, Germany) was used.

TEM/EDX analyses were performed on a conventional microscope JEM 2100 (Jeol, Japan) operated at 200 kV and equipped with EDX spectrometer. Prior to TEM analyses, the specimens were coated by 3-nm layer of carbon to improve surface electron conductivity performed. PECS 68s equipment (Gatan inc., Pleasanton, CA, USA) was used for this purpose. For technical reasons, the TEM analysis was performed only for the final sample prepared by laboratory milling (LM_{\max}).

The Mössbauer spectra of both powdered and hot-pressed samples were collected at room temperature (RT) and at 4.2 K in standard transmission geometry with a constant acceleration mode of the γ -ray source kept at RT. The ^{57}Fe Mössbauer spectra were acquired with the $^{57}\text{Co/Rh}$ source, the calibration of velocities and isomer shifts of ^{57}Fe was performed with respect to a calibration α -Fe foil at room temperature. The $\text{Ca}^{119\text{m}}\text{SnO}_3$ source, sharing the same Mössbauer drive as the $^{57}\text{Co/Rh}$ source, was used to collect ^{119}Sn Mössbauer spectra. Thus the calibration of velocities (only with opposite sign) could be related to the ^{57}Fe spectrum of the α -Fe foil, which offers higher precision over the velocity scale than SnO_2 due to the α -Fe six-line spectrum. The isomer shifts of ^{119}Sn spectra are related to SnO_2 at RT. The low-temperature spectra were measured in zero magnetic fields and at 6 T, in a liquid-helium bath cryostat by Janis Research (Lake Shore Cryotronics, Inc., USA) with the orientation of the applied field perpendicular to the direction of γ -rays. The spectra were evaluated by using the Confit software [46].

Bulk samples for thermoelectric characterization were obtained by hot pressing of powders in a graphite die at 723 K and 60 MPa for 1 h. Diamond wire saw was used to cut the pellets, both above 90% of theoretical density, into smaller pieces for subsequent analysis. One bar (about $1.5 \times 1.5 \times 7 \text{ mm}^3$) was used to determine the electrical resistivity ρ , Seebeck coefficient S and thermal conductivity κ between 300 and 2 K employing the TTO module of the PPMS instrument (Quantum Design, Inc., USA). A similar bar was used to determine ρ and S between 300 and 600 K using a custom four-probe measurement system in N_2 atmosphere. Finally, a flat sample (about $6 \times 6 \times 1.5 \text{ mm}^3$) was used to determine the thermal conductivity in a similar temperature range from the formula $\kappa = \rho \cdot a \cdot c_p$, where ρ is the density

determined experimentally, and a and c_p are diffusivity and specific heat, respectively, measured using the LFA 467 (Netzsch, Germany) instrument for light flash analysis.

Results and discussion

Optimization of mechanochemical synthesis via Taguchi design and response modelling

To obtain product through mechanochemical experiments, high-energy mill as a mechanochemical reactor is needed [17]. Multiparameter approach to propose the milling experiments encompasses usually several variables like milling time (t_m), revolutions of the mill (n), and ball-to-powder ratio (b/p). When constant amount of balls (b) is applied, the amount of powder (m) can be used as variable. These experiments can be performed by a *classical design of experiments* where the variables are fixed and the only one selected is being changed. However, this approach is subjective because the selected variable is based on personal decision of experimenter. More sophisticated is the so-called statistical design of experiments (DOE). Among DOE methods, the Taguchi method has an inevitable place [47] due to the possibility to reduce the number of experiments in comparison with the full factorial design [47, 48]. This enables finding the optimum conditions in a relatively quick manner. The experimental conditions of high-energy ball milling has been also optimized by Taguchi design more times (e.g. in [49–51]).

In our experiments, we tried to optimize conditions of laboratory planetary milling by Taguchi methodology. The variables t_m , n and m were used as inputs and the measured saturation magnetization M and the corresponding conversion degree α calculated by Eq. (2) as outputs. The detailed description of this part of work is provided in the ESI (Section S1.a). The optimization results showed that the specific focus should be given to milling time. As a consequence, the second round of experiments with the milling time t_m prolonged up to 120 min was performed and the progress of the reaction was investigated via X-ray diffraction and saturation magnetization measurements.

Phase and elemental analysis after mechanochemical synthesis

Phase analysis versus milling time

The quaternary Cu–Fe–Sn–S system represents a great variety of possible sulphide structures. Even in ternary Cu–Sn–S system around 20 phases are possible [6]. In ternary Cu–Sb–S system 4 phases were identified [14]. Some

of them were already synthesized by high-energy milling as mentioned in Introduction.

The XRD patterns of powders after co-milling of Cu, Fe, Sn and S mixture of precursors in both types of mills are illustrated by Figs. 1 and 2. All precursors were weighed stoichiometrically to obtain chatkalite $\text{Cu}_6\text{FeSn}_2\text{S}_8$ as expectable main product of the mechanochemical synthesis.

The progress of synthesis by laboratory milling is illustrated in Fig. 1a. Milling times for 5–120 min have been applied. Already in the very early stages of reaction (5–20 min) the expected chatkalite $\text{Cu}_6\text{FeSn}_2\text{S}_8$ is present. However, also stannite $\text{Cu}_2\text{FeSnS}_4$ as the further quaternary sulphide is detected. It seems that at the beginning of synthesis stannite is prevailing over chatkalite, however, the stannite \rightarrow chatkalite transformation occurs with increasing amount of milling energy, as can be traced down by the shift of the diffraction peaks to higher 2θ values (see the zoomed region shown in Fig. 1b). According to our previous paper aimed at stannite mechanochemical synthesis, this phase is formed very fast with the first step being a mechanically induced self-propagating reaction (MSR) between copper and sulphur [32]. Covellite CuS is also present in Fig. 1 at shorter milling times. It was observed that CuS itself can be formed within a second range in a laboratory mill and in some cases, its synthesis can be done via a MSR pathway [52, 53]. However, the overall picture of milling at shorter milling times is even more complicated by the presence of non-consumed tin Sn and herzenbergite SnS . The prior formation of binary sulphides as intermediates of mechanochemical synthesis of the ternary and quaternary sulphides is in accord with findings in recent works [14, 35].

In the later stages of reaction (45–120 min) only quaternary sulphides chatkalite $\text{Cu}_6\text{FeSn}_2\text{S}_8$ and stannite

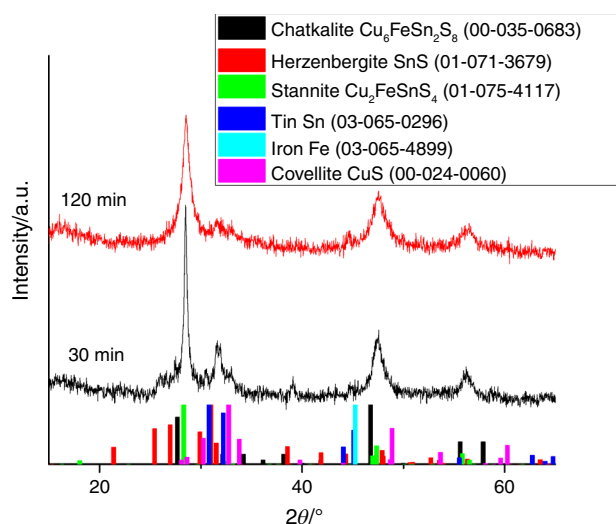


Fig. 2 XRD patterns of powders after milling in an industrial mill (milling times are in the patterns)

$\text{Cu}_2\text{FeSnS}_4$ together with non-consumed iron are detected. CuS is no more present as it represents a reactive precursor for progress of consecutive syntheses of the mentioned sulphides. The diffractions of tin are also absent, because it reacts with sulphur forming SnS which belongs among volatile sulphides [54]. However, the intensity of SnS diffraction peaks is most probably too low to be detected by XRD. Moreover, we suppose that part of SnS together with the non-consumed sulphur volatilize during milling at higher energy input (higher milling times).

Based on products identified by XRD measurements a sequence of reactions in the system under study can be outlined:

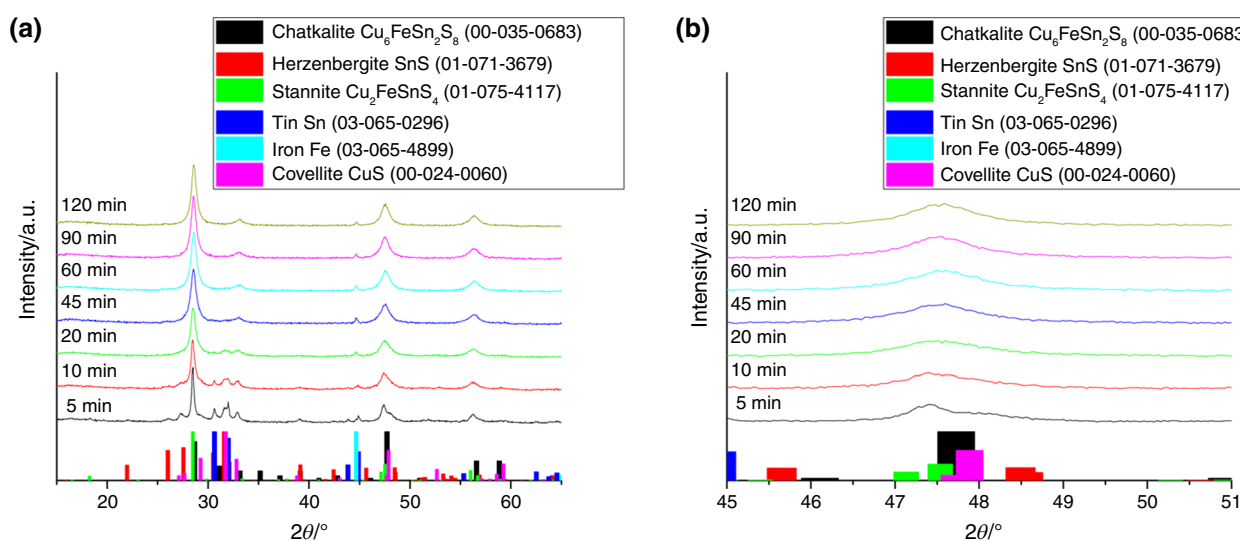
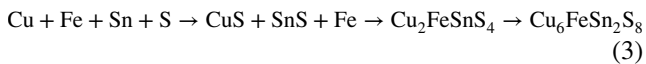


Fig. 1 **a** XRD patterns of powders after milling in a laboratory mill (milling times are in the patterns), **b** zoomed region between $2\theta = 45\text{--}51$ deg



Kinetics of the mechanochemical synthesis is described later.

Industrial milling was performed for two milling times 30 and 120 min and the corresponding XRD patterns are provided in Fig. 2. The choice of the mentioned durations of high-energy treatment in an industrial mill was selected with the intention to study mechanochemical synthesis in a short- (30 min) and long-term (120 min) process, which could yield different effects (such as increasing specific surface area in the former case and agglomeration in the latter one). In principle, the same patterns as in Fig. 1a were obtained. However, the progress of reaction is not so great as in the case of laboratory milling. Besides chatkalite and stannite, also precursors of synthesis and binary products characteristic for shorter milling times in laboratory milling (Fig. 1a) are present in both industrially milled samples.

Chemical composition versus milling time

To understand the distribution of the individual elements in powders after the mechanochemical treatment, EDX mapping and SEM analysis was performed for the milled samples. The data were obtained by averaging of 2–4 measurements. The results are summarized in Table 1. In lower part of the Table theoretical composition of chatkalite $\text{Cu}_6\text{FeSn}_2\text{S}_8$ and stannite $\text{Cu}_2\text{FeSnS}_4$ is given.

Based on the EDX measurements in a SEM mode, the final elemental composition for all samples is closer to chatkalite than stannite. This statement is mostly valid for all four elements. However, this is more appropriate valid for samples milled for longer times where mainly chatkalite and stannite are formed next to the non-consumed iron, see Figs. 1 and 2. Moreover, it has to be taken into account that

Table 1 SEM/EDX analysis of the milled samples and comparison to theoretical values of chatkalite and stannite

Milling mode	Milling time/min	Atomic %			
		Cu	Fe	Sn	S
Laboratory milling	5	52.73	2.84	7.36	37.08
	20	38.01	2.91	11.48	47.06
	45	36.05	4.60	11.69	47.67
	60	42.46	4.39	10.24	42.92
	90	42.60	4.51	10.50	42.40
	120	42.62	4.27	9.23	43.90
Industrial milling	30	44.90	4.36	10.19	40.55
	120	37.37	5.91	10.45	46.28
Chatkalite $\text{Cu}_6\text{FeSn}_2\text{S}_8$	–	35	6	12	47
Stannite $\text{Cu}_2\text{FeSnS}_4$	–	25	12.5	12.5	50

the initial elemental composition used for the synthesis was designed to exactly match that of chatkalite.

Combination of SEM, EDX and elemental mapping for selected samples is given in the ESI (Fig. S1.1 and 1.2). Appropriate harmony between experimental and theoretical values for both selected samples is documented. SEM photographs show more uniform distribution of particles for laboratory milling (Fig S1.1A) in comparison with the sample synthesized by industrial milling (Fig. S1.2A). In the first case the most particles are agglomerates of nanoparticles approximately 10–20 μm in size. However, also larger particles with smooth surface and irregular habitus next to the small ones can be identified in the second case (Fig. S1.2A). Elemental mapping confirms homogeneous distribution of Cu, Sn and S. However, for Fe mapping except of regular picture also “shining” particles can be seen illustrating the appearance of non-consumed iron. This picture is more pronounced for sample prepared by industrial milling.

Kinetics of mechanochemical solid state synthesis

Magnetization versus milling time

A set of samples milled for 5–120 min in a laboratory mill was measured by a magnetometer from which the values of magnetization M in dependence on applied magnetic field were obtained (Fig. 3). Furthermore, the figure shows values of M of two hot pressed samples. Monotonous decrease in magnetization for all powder samples with setting values of the saturation magnetization M_s at 5 T was detected. However, a relatively large difference in M_s values between the non-milled sample and the milled ones was documented. In the first case where Fe was present in elemental non-reacting form $M_s = 13.79 \text{ A m}^2 \text{ kg}^{-1}$ while these values for milled samples were in between

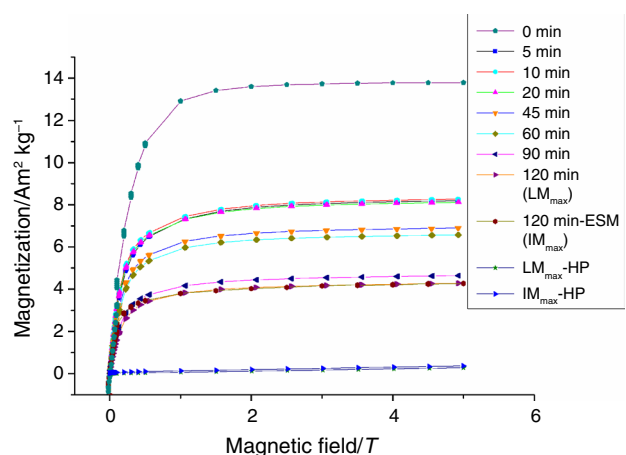


Fig. 3 Magnetization versus magnetic field for products of mechanochemical synthesis (HP stands for samples after hot pressing)

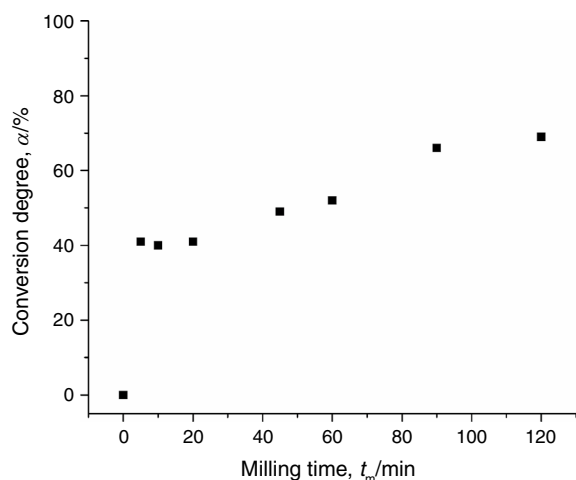


Fig. 4 Conversion degree, α versus milling time, t_M for products of mechanochemical synthesis performed in a laboratory mill

8.27 and 4.27 A m² kg⁻¹, respectively. This trend documents the rapid consumption of strongly magnetic Fe during mechanochemical reaction (5–120 min) by its incorporation into less-magnetic products. Hot pressing (HP) led to almost complete conversion of elemental Fe. This consolidation method thus represents not only mechanical homogenization but also chemical tool to finish the solid state reaction.

Based on magnetization data obtained for the lab-scale synthesis the conversion degree α of synthesis was calculated using Eq. (2). The dependence of the corresponding data on the milling time is given in Fig. 4. In general, two regimes appeared: first a sharp increase of α at the beginning of milling up to $t_M \leq 20$ min and then a gradual increase up till $t_M = 120$ min. Totally, the maximum value of $\alpha = 69\%$ was calculated for sample milled for 120 min in a laboratory mill.

Detailed study of the optimum samples

The appearance of non-consumed iron and two quaternary sulphides in products of mechanochemical synthesis induced the necessity to broaden portfolio of identification methods. Mössbauer spectroscopy (to identify iron oxidation states), EDX and TEM analysis (to bring more light on the presence of chatkalite and stannite phases as well as the size of nanoparticles) were applied. The samples milled for 120 min in laboratory (LM_{max}) and industrial (IM_{max}) mode were selected for the detailed characterization.

TEM and EDX analysis of LM_{max} sample

Low-magnification TEM image of the LM_{max} sample is shown in Fig. 5a. It reveals that the sample is composed

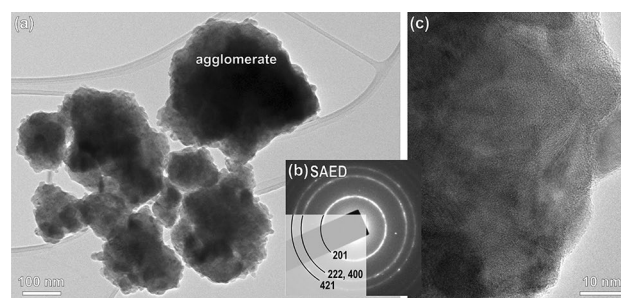


Fig. 5 **a** TEM image and **b** SAED pattern of the LM_{max} sample. The rings belong to chatkalite, Miller indices of the lattice planes are marked on the diffraction pattern. **c** HRTEM image

of few hundred nanometer large agglomerates of smaller particles. Selected area electron diffraction (SAED) pattern (Fig. 5b) contains three clear diffraction rings confirming that the sample is crystalline. The fine size of diffraction dots comprising the rings suggests that the size of the crystallites is in the nanometer range. The analysis of the d values confirms that the sample is chatkalite. Crystallinity and size of the crystallites was confirmed also by high-resolution TEM (Fig. 5c). The images show tightly packed nanosized crystallites with sizes in up to few tens of nanometres. Local chemical composition of the sample was analysed by EDX. The analyses were performed by acquisition of single analyses in thin parts of the sample, the positions of seven EDS measurements are shown on the image in Supplementary Information. Quantification of Cu, Fe, Sn and S and the Cu/S ratio for the EDX analyses are given in Table 2. The results suggest that the chemical analysis of the sample is fairly homogenous. The comparison with theoretical compositions of chatkalite Cu₆FeSn₂S₈ and stannite Cu₂FeSnS₄ shows that the composition of the sample is in better agreement with chatkalite. Namely, the amount of sulphur and copper almost exactly matches the theoretical amount, but the stoichiometry is deficient in iron (for ~33%) and rich in tin (for ~19%). This suggests easier incorporation of tin into the crystal structure. On the other hand, the opposite content of Fe²⁺ and Sn⁴⁺ is likely to occur in order to preserve the charge balance of the compound. Due to the proper amounts of S and Cu, also the experimental Cu/S ratio (0.8) is close to the expected value for chatkalite (0.75) and is significantly different from the one of stannite (0.5).

Mössbauer spectroscopy and Rietveld refinement

To resolve the oxidation states of Fe and Sn, which would facilitate the phase analysis, and to monitor the phase transformation upon hot pressing in the LM_{max} and IM_{max} samples from two complementary local viewpoints, we employed ⁵⁷Fe and ¹¹⁹Sn Mössbauer spectroscopy, which uses the resonating nuclei as local probes and does not

Table 2 TEM/EDX analyses of the laboratory milled LM_{max} sample

No. of analysis	Cu	Fe	Sn	S	Cu/S
	Atomic %				
1	31.7	3.9	16.8	47.6	0.67
2	42.9	3.6	10.3	43.2	0.99
3	33.9	4.4	15.0	46.6	0.73
4	33.4	4.5	15.0	47.0	0.71
5	37.6	3.7	12.9	45.9	0.82
6	40.4	3.3	14.1	42.2	0.96
7	34.0	5.2	14.3	46.5	0.73
8	37.7	3.4	13.7	45.2	0.83
9	36.5	3.3	14.3	45.9	0.80
Average	36.5	3.9	14.0	45.6	0.80
Chatkalite Cu ₆ FeSn ₂ S ₈	35.3	5.9	11.8	47.1	0.75
Stannite Cu ₂ FeSnS ₄	50.0	12.5	25.0	12.5	0.50

require a long-range ordering. The room temperature (RT) spectra of both the LM_{max} powder and pellet are shown in Fig. 6. The spectra acquired at 4.2 K, spectra of IM_{max}, hyperfine parameters of the individual components of the fits, and more detailed comments on the phase analysis are provided in the section S2 in the Supporting Information (SI). The residual α -Fe (23–26% of Fe atoms) in the powders completely reacted during the hot pressing and was not present in the pellets. The RT spectra show a minor doublet (D_1 and D_4) with the intensity of several percent that can be ascribed to the high-spin divalent iron, which is expected for stoichiometric chatkalite and stannite phases [55]. However, Fe^{3+} largely dominates in the samples ($D_{2,3}$ and $D_{5,6}$). At the liquid-helium temperature, the present iron-containing phases are magnetically ordered, and, importantly, the samples likely do not contain polymorphs of iron oxides or oxy-hydroxides, although some trace amounts cannot be excluded due to the lower quality of the spectra. The ^{119}Sn Mössbauer spectra evidenced the exclusive presence of Sn^{4+} in the samples, whereas for the IM_{max} powder, where in addition to tetravalent tin, also up to 17% of Sn occurred in the divalent form (Fig. S2.2 in the SI). The majority of Sn was incorporated into sulfide phases (doublets D_{Sn1} – D_{Sn4}), nevertheless, both samples contained cassiterite (SnO_2 , D_{SnO} doublet), the content of which increased significantly by hot pressing.

Figure 7 shows the X-ray diffraction pattern of powdered material of the hot-pressed pellets of the LM_{max} and IM_{max} samples, which were used for the measurement of thermoelectric properties (as will be shown later). The presence of two major phases was confirmed for both samples. The dominant phase is stannite (cca 60 vol%), and the second major phase is chatkalite (cca 30 volume%). Additional minor phases were identified as SnO_2 and $Cu_{1,6}S$ (each approximately in 5 vol%). The structural features of stannite

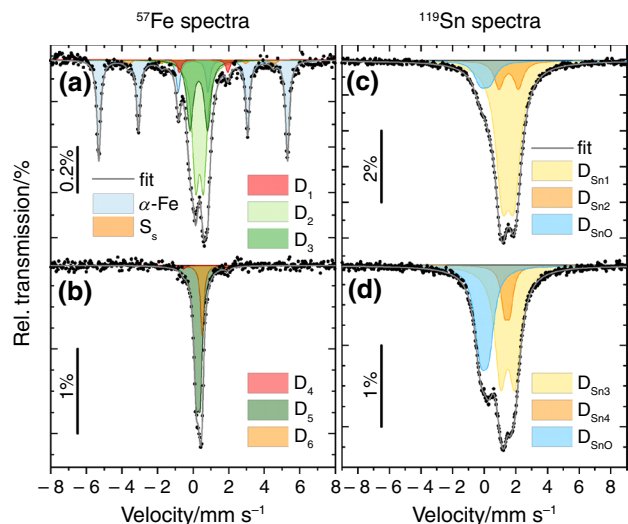
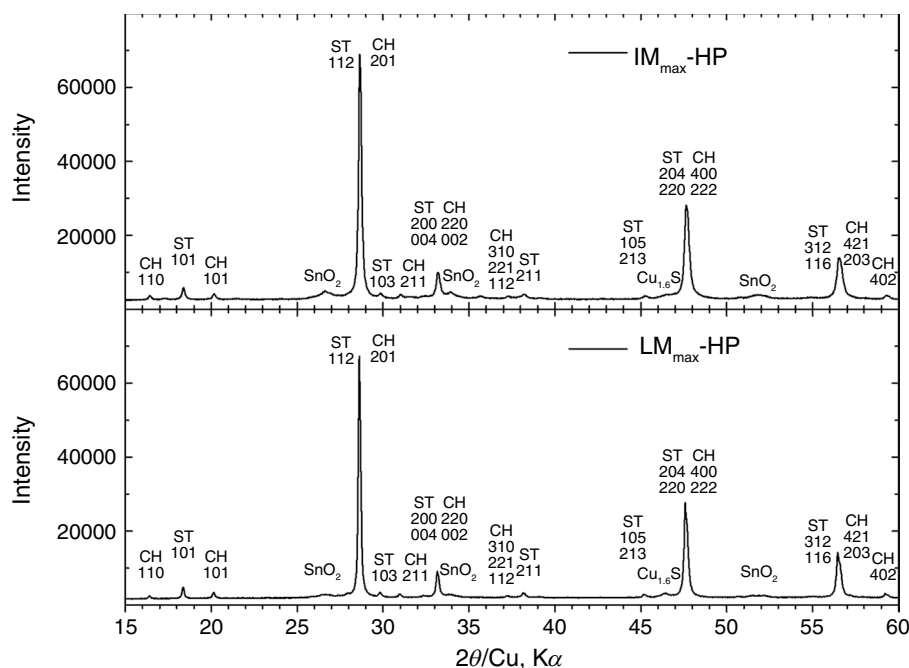


Fig. 6 Room-temperature Mössbauer spectra of the LM_{max} sample: ^{57}Fe spectra of the powder (a), the pellet (b); ^{119}Sn spectra of the powder (c) and the pellet (d). The vertical scale denotes the effect of the measured spectra

(Cu_2FeSnS_4) and chatkalite ($Cu_6FeSn_2S_8$) phases are illustrated in Fig. S3.1 in SI, together with another similar phase mawsonite ($Cu_6Fe_2SnS_8$). For the sake of comparison, the structures are displayed in a common supercell (approximately $10.8 \times 10.8 \times 5.4$ Å). It can be seen that these phases are crystallographically very similar, and their diffraction patterns share the main peaks and only differ by less intensive peaks. This extensive peak overlap makes the structural refinement of the multi-phase samples difficult. Therefore, we have only determined the stoichiometry and structural details for stannite, whereas we kept the ideal stoichiometry for the second major phase chatkalite in the refinement. The stoichiometry of the stannite phase was refined as $Cu_2Fe_{1,2}Sn_{0,6-0,2}S_4$. The difference from the ideal stoichiometry is the excess of Fe at the expense of Sn and a small number of vacancies on cation sites. Supposing typical valencies of Cu^{1+} , Sn^{4+} and S^{2-} , the refined stoichiometry gives the valency Fe^{3+} , instead of Fe^{2+} corresponding to the ideal stoichiometry. The determined valency Fe^{3+} for stannite is in accordance with the Mössbauer spectroscopy results. The stoichiometry of chatkalite was not refined, but the Fe^{3+} valency could be also possibly explained by vacancies on Sn sites, such as $Cu_6FeSn_{1,75-0,25}S_8$. The presence of vacancies on Sn sites is in accordance with the observation of SnO_2 phase as an impurity.

In general, hot pressing served not only as a physical densification tool but also as chemical reaction tool, as the present compounds have changed in comparison with the as-received powders after milling. Namely, the transformation of chatkalite into stannite phase was observed.

Fig. 7 X-ray diffraction patterns of hot-pressed pellets. Indexes of major phases stannite (ST) and chatkalite (CH) and peaks of minor phases are indicated. Agreement factors of Rietveld refinement for IM_{\max} -HP: $R_p = 2.13\%$, $R_{wp} = 2.85\%$, $\chi^2 = 2.63\%$, for LM_{\max} -HP: $R_p = 1.97\%$, $R_{wp} = 2.58\%$, $\chi^2 = 1.98\%$



Thermoelectric performance

Thermoelectric properties of LM_{\max} and IM_{\max} samples can be seen in Fig. 8. Both samples display semiconducting behavior as evidenced by the temperature dependence of electrical resistivity and moderate values of Seebeck coefficient. Seebeck coefficient is positive in the whole temperature range, suggesting that holes act as the main charge carriers. Its diffusive character is evidenced by the nearly linear temperature dependence which tends to zero at 0 K. In line with the electronic structure calculations detailed in Supplementary Information (Fig. S2.1), the measurements suggest that the Fermi level is close to the top of the valence band and electrical properties are governed by Cu–S states.

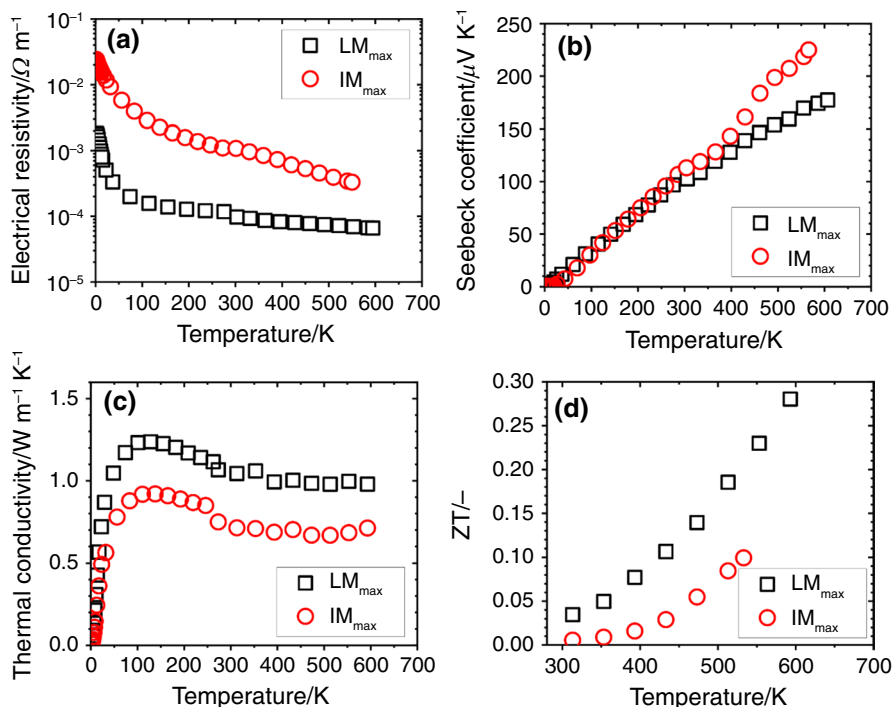
The Seebeck coefficient (Fig. 8b) of the two samples is strikingly similar, in contrast with their electrical resistivities which differ by an order of magnitude (Fig. 8a). A reasonable explanation is a difference in the amount of interfaces and boundaries in the two samples induced by high-energy milling. This impedes electrical transport and increases electrical resistivity in the IM_{\max} sample. To a lesser extent, thermal transport is also influenced, leading to lower thermal conductivity in this case (see Fig. 8c). Seebeck coefficient is generally much less sensitive to such disruptions, explaining its similar values. Measured thermal conductivity κ is dominated by lattice thermal conductivity; the electronic part, estimated using the Wiedemann-Franz law, does not exceed $0.2 \text{ W m}^{-1} \text{ K}^{-1}$. Thermal conductivity is around $1 \text{ W m}^{-1} \text{ K}^{-1}$ in most of the temperature range, which is a low value favorable for thermoelectric applications.

The maximum value of the calculated thermoelectric figure of merit $ZT = 0.27$ was obtained at 600 K for the LM_{\max} sample (Fig. 8d). In the case of IM_{\max} sample, the maximum ZT equals to about half of that, mainly because of the higher electrical resistivity.

In summary, comparison of the transport parameters for laboratory milled LM_{\max} and industrially milled IM_{\max} samples is illustrated by Fig. 8a–c from data of which the corresponding figure of merit ZT was calculated (Fig. 8d).

As stated in previous paragraph, the main difference is in the electrical resistivity where corresponding values for industrially milled sample are one order magnitude higher in comparison with the laboratory milled counterpart. The explanation can be hidden in different supply of mechanical energy and corresponding wear of balls during mechanochemical synthesis. As stated in Supplementary Information (Section S1a), high-energy milling is a multifactorial event where different processing parameters play a decisive role, as defined by regression Eq. (4). In our case three parameters were studied, i.e. milling time t_m , revolutions of the mill n and mass of milled sample m_s . Milling time was constant for both milling modes ($t_m = 120 \text{ min}$). According to Eq. (4), the most influential parameter on course of synthesis (by constant mass of milling balls m_B) was the mass of sample m_s . However, in our case values of m_B and m_s were different. When comparing the applied conditions for laboratory milling their ratio was $m_B/m_s = 135 \text{ g}/10 \text{ g} = 13.5$ in contrary to industrial milling where this value was $m_B/m_s = 35,000 \text{ g}/100 \text{ g} = 350$, respectively. It follows that during industrial milling, the impact of balls on milled sample is $350:13.5 = 25.9$ -times more intensive. This factor is

Fig. 8 Temperature dependence of **a** electrical resistivity, **b** Seebeck coefficient, **c** thermal conductivity, and **d** figure of merit ZT of hot-pressed samples LM_{max} and IM_{max}



supported by revolutions of the mill which also characterizes intensity of supplied milling energy and is higher for industrial milling ($n=960 \text{ min}^{-1}$) in comparison with laboratory milling (500 min^{-1}). The accompanying sign for each mechanochemical event is wear of milling balls [17, 56]. In our case the applied balls were from tungsten carbide WC. According to chemical analysis (dissolution in HNO_3) the estimated content of W in milled samples was 0.0114% and 0.0192% for LM_{max} and IM_{max}, respectively. WC is characterized by high electrical resistivity $2 \times 10^7 \text{ } \Omega \text{ m}$ which is significantly higher than the values presented in Fig. 8a. It follows from the presented data, that the higher wear can be responsible for higher electrical resistivity in samples prepared by industrial milling.

Differences in the thermal conductivity data between industrial and laboratory milling can be observed in Fig. 8c. In this case several factors must be borne in mind. The presence of WC and nanosized character of produced powders (see Fig. 5 for laboratory milling) belong to the most important ones. They contribute to enhanced grain and phase boundaries formation and, as a consequence of it, to a higher scattering of phonons which are responsible for reduced values of thermal conductivity. These phenomena are more influential for industrial milling as evidenced in Fig. 8c.

Conclusions

We successfully demonstrated the possibility to engage elemental precursors Cu, Fe, Sn and S in a solid-state mechanochemical synthesis to produce corresponding quaternary sulphides. The product after milling was further processed by hot press compacting technique to consolidate the powder. In this strategy it was possible to prepare a nanobulk chatkalite $\text{Cu}_6\text{FeSn}_2\text{S}_8$ /stannite $\text{Cu}_2\text{FeSnS}_4$ composite containing minor amounts of cassiterite SnO_2 and geerite $\text{Cu}_{1.6}\text{S}$. The TEM/EDX study documented tightly packed nanosized crystallites approximately 10–20 nm in size and dominating chatkalite phase. Such original synthetic approach was applied for the first time using a laboratory planetary and an industrial eccentric vibration mills, respectively. Especially application of industrial mill paved the way of scaling-up the synthesis process.

Using magnetometry to follow the kinetics of synthesis, the non-consumed Fe as a marker was applied. The mechanochemical reaction proceeds as a multistep process comprising binary sulphides SnS and CuS at the beginning and quaternary chatkalite/stannite nanocomposite at the end of synthesis. The strong magnetic Fe is consumed and incorporated into less magnetic quaternary sulphides.

The detailed Mössbauer study on hot-pressed samples unveiled that iron is present in the composite in the 3+ oxidation state and only very minor part (<2%) could be detected as Fe^{2+} . Tin is present in the 4+ oxidation state. These facts were projected into phase and chemical composition, as evidenced also by XRD and magnetic data. It was

further confirmed that the final hot pressing process leads to the incorporation of residual iron (remaining in the mechanochemically synthesized nanopowder) into the quaternary sulphide composite while tin remains in a lesser extent in a form of SnO₂ precipitates.

Considering the structural and chemical nearness of chatkalite and stannite structures, we were not able to specify the exact composition of the as-synthesized nanopowders, however, for sintered pellets we succeeded to determine the approximate phase composition. As the sulphur-containing phases are depleted of Sn, having important impact on Fe valency and vacancies in the structure, the main phase (60%) in the pellet and the powder was identified as vacancies-containing stannite with modified stoichiometry (Fe > Sn), namely Cu₄Fe_{2.4}Sn_{1.2}S₈. This phase dominates the electrical and thermoelectric properties. As the second most abundant phase (30%) we identified chatkalite. The existence of Fe³⁺, on the contrary to ideal Fe²⁺, is explained by a small number of vacancies on Sn sites.

Based on electronic structure calculations the most distinct density of electronic states at Fermi level is linked with Cu states in chatkalite and stannite. This explains the positive (hole-like) thermopower and high electrical conductivity associated with highly dispersive bands. The diffusive thermopower represented by utmost linear temperature dependence is thus likely dominated by strongly hybridized Cu–S states at Fermi level. This fact is important when dealing with likely different than theoretical 2+ valence of iron in stannite and chatkalite. We explain the observed electrical properties by the dominating role of Cu3d utmost filled band strongly hybridized with sulphur.

Considering thermoelectric performance, several new findings were identified. Thermal conductivity is dominated by phonons and is very low due to multiphase nature of composite material, low thermal conductivity of respective phases tied to their complex structure and the phonon reflection due to further present impurities. The role of small grain/particle size in thermal conductivity is likely less important. Based on the thermoelectric measurements the calculated figure-of-merit reached value $ZT = 0.27$ at 600 K which is somewhat lower than that previously published for a mawsonite/stannite composite where $ZT = 0.51$ at 623 K [31]. The difference is due to a higher thermal conductivity of chatkalite/stannite composite studied in this work.

The experimental material presented in this paper is in accordance with the aims defined in the introduction. Non-traditional approach to apply magnetometry for the study of the kinetics of solid-state mechanochemical synthesis can be accepted as the experimental novelty. The successful carrying out of the synthesis in an industrial mill represents a valuable approach to manifest the novelty indispensable for future applications. In general, the paper presents novel

perspectives for the study of environmentally acceptable high-performance thermoelectric materials.

Supplementary Information The online version contains supplementary material available at <https://doi.org/10.1007/s10973-024-12931-0>.

Acknowledgements This work was supported by the Slovak Grant Agency (projects VEGA 2/0112/22 and 2/0036/23). N.D. acknowledges financial support from the Slovenian Research Agency in the frame of research program P1-0091. The support of COST Action CA18112 MechSustInd (www.mechsustind.eu), supported by the COST Association (European Cooperation in Science and Technology, www.cost.eu) is also acknowledged. We acknowledge the financial support of the Czech Science Foundation (project 18-12761S). Experiments were performed in MGML (mgml.eu), which is supported within the program of Czech Research Infrastructures (project no. LM2018096). Computational resources were supplied by the e-INFRA CZ project (ID: 90254), supported by the Ministry of Education, Youth and Sports of the Czech Republic. The experiments performed at the Institute of Physics were also supported by the Operational Program Research, Development and Education financed by the European Structural and Investment Funds and by the Czech Ministry of Education, Youth and Sports, project number CZ.02.1.01/0.0/0.0/16_019/0000760 (SOLID21).

Funding Open access funding provided by The Ministry of Education, Science, Research and Sport of the Slovak Republic in cooperation with Centre for Scientific and Technical Information of the Slovak Republic.

Open Access This article is licensed under a Creative Commons Attribution 4.0 International License, which permits use, sharing, adaptation, distribution and reproduction in any medium or format, as long as you give appropriate credit to the original author(s) and the source, provide a link to the Creative Commons licence, and indicate if changes were made. The images or other third party material in this article are included in the article's Creative Commons licence, unless indicated otherwise in a credit line to the material. If material is not included in the article's Creative Commons licence and your intended use is not permitted by statutory regulation or exceeds the permitted use, you will need to obtain permission directly from the copyright holder. To view a copy of this licence, visit <http://creativecommons.org/licenses/by/4.0/>.

References

- Baláž P, Baláž M, Achimovičová M, Bujňáková Z, Dutková E. Chalcogenide mechanochemistry in materials science: insight into synthesis and applications (a review). *J Mater Sci*. 2017;52:11851–90.
- Qiu PF, Shi X, Chen LD. Cu-based thermoelectric materials. *Energy Storage Mater*. 2016;3:85–97.
- Powell AV. Recent developments in Earth-abundant copper-sulfide thermoelectric materials. *J Appl Phys*. 2019;126:100901.
- Wei TR, Qin YT, Deng TT, Song QF, Jiang BB, Liu RH, Qiu PF, Shi X, Chen LD. Copper chalcogenide thermoelectric materials. *Sci China Mater*. 2019;62:8–24.
- Olatunde OC, Onwudiwe DC. Stoichiometric phases and mechanism of crystal phase selectivity of copper-based ternary sulphides. *Mater Sci Semicond Process*. 2021;125:105627.
- Kumar VP, Lemoine P, Carnevali V, Guelou G, Lebedev OI, Boullay P, Raveau B, Al Orabi RA, Fornari M, Prestipino C, Menut D, Candolfi C, Malaman B, Juraszek J, Guilmeau E. Ordered sphalerite derivative Cu₃Sn₂S₇: a degenerate semiconductor with

- high carrier mobility in the Cu–Sn–S diagram. *J Mater Chem A*. 2021;9:10812–26.
7. P. Lemoine, G. Guelou, B. Raveau, E. Guilmeau, Crystal Structure Classification of Copper-Based Sulfides as a Tool for the Design of Inorganic Functional Materials, *Angew. Chem. Int. Ed.* 2022; 61:e202108686.
 8. Trajic J, Romcevic M, Petrovic M, Gilic M, Balaz P, Zorkovska A, Romcevic N. Optical properties of the mechanochemically synthesized $\text{Cu}_2\text{FeSnS}_4$ (stannite) nanocrystals: Raman study. *Opt Mater*. 2018;75:314–8.
 9. Trajic J, Romcevic M, Paunovic N, Curcic M, Balaz P, Romcevic N. Far-infrared study of the mechanochemically synthesized $\text{Cu}_2\text{FeSnS}_4$ (stannite) nanocrystals. *Infrared Phys Technol*. 2018;90:66–9.
 10. Hegedus M, Achimovicova M, Hui HJ, Guelou G, Lemoine P, Fourati I, Juraszek J, Malaman B, Balaz P, Guilmeau E. Promoted crystallisation and cationic ordering in thermoelectric $\text{Cu}_{26}\text{V}_2\text{Sn}_6\text{S}_{32}$ colusite by eccentric vibratory ball milling. *Dalton Trans*. 2020;49:15828–36.
 11. Baláz P, Hegedüs M, Baláz M, Daneu N, Šiffalovič P, Bujňáková Z, Tóthová E, Tešínský M, Achimovičová M, Briančin J, Dutková E, Kaňuchová M, Fabián M, Kitazono S, Dobrozhan O. Photovoltaic materials: $\text{Cu}_2\text{ZnSnS}_4$ (CZTS) nanocrystals synthesized via industrially scalable, green, one-step mechanochemical process. *Prog Photovoltaics*. 2019;27:798–811.
 12. Hegedüs M, Baláz M, Tešínský M, Sayagués MJ, Šiffalovič P, Kruľáková M, Briančin J, Fabián M. Scalable synthesis of potential solar cell absorber Cu_2SnS_3 (CTS) from nanoprecursors. *J Alloys Compd*. 2018;768:1006–10015.
 13. Levinsky P, Hejtmanek J, Knizek K, Pashchenko M, Navratil J, Masschelein P, Dutkova E, Balaz P. Nanograined n- and p-type chalcopyrite CuFeS_2 prepared by mechanochemical synthesis and sintered by SPS. *Acta Phys Pol A*. 2020;137:904–7.
 14. Baláz P, Guilmeau E, Daneu N, Dobrozhan O, Baláz M, Hegedus M, Barbier T, Achimovičová M, Kaňuchová M, Briančin J. Tetrahedrites synthesized via scalable mechanochemical process and spark plasma sintering. *J Eur Ceram Soc*. 2020;40:1922–30.
 15. Balaz P, Balaz M, Dutkova E, Hegedus M, Rajnak M, Knizek K, Hejtmanek J, Navratil J, Achimovicova M, Briančin J. Magnetization as an effective tool for kinetics evaluation in mechanochemical synthesis of chalcopyrite CuFeS_2 . *Acta Phys Pol A*. 2020;137:647–9.
 16. Baláz P, Achimovičová M, Baláz M, Chen K, Dobrozhan O, Guilmeau E, Hejtmanek J, Knížek K, Kubíčková L, Levinský P, Puchý V, Reece MJ, Varga P, Zhang R-Z. Thermoelectric CuS-based materials synthesized via a scalable mechanochemical process. *ACS Sust Chem Eng*. 2021;9:2003–16.
 17. Baláz P. Mechanochemistry in nanoscience and minerals engineering. Berlin Heidelberg: Springer; 2008.
 18. Frišćić T. New opportunities for materials synthesis using mechanochemistry. *J Mater Chem*. 2010;20:7599–605.
 19. Šepelák V, Becker KD. Mechanochemistry: from mechanical degradation to novel materials properties. *J Korean Ceram Soc*. 2012;42:19–28.
 20. Frišćić T, Halasz I, Beldon PJ, Belenguer AM, Adams F, Kimber SAJ, Honkimäki V, Dinnebir RE. Real-time and in situ monitoring of mechanochemical milling reactions. *Nature Chem*. 2013;5:145–145.
 21. Baláz P, Achimovičová M, Baláz M, Billik P, Cherkezova-Zhelleva Z, Criado JM, Delogu F, Dutková E, Gaffet E, Gotor FJ, Kumar R, Mitov I, Rojac T, Senna M, Streletskii A, Wiczorek-Ciurowa K. Hallmarks of mechanochemistry: from nanoparticles to technology. *Chem Soc Rev*. 2013;42:7571–637.
 22. Beyer MK, Clausen-Schaumann H. Mechanochemistry: the mechanical activation of covalent bonds. *Chem Rev*. 2005;105:2921–48.
 23. Do JL, Frišćić T. Mechanochemistry: a force of synthesis. *ACS Central Sci*. 2017;3:13–9.
 24. Moores A. Bottom up, solid-phase syntheses of inorganic nanomaterials by mechanochemistry and aging. *Curr Opin Green Sust Chem*. 2018;12:33–7.
 25. Tan D, Garcia F. Main group mechanochemistry: from curiosity to established protocols. *Chem Soc Rev*. 2019;48:2274–92.
 26. Mucsi G. A review on mechanical activation and mechanical alloying in stirred media mill. *Chem Eng Res Des*. 2019;148:460–74.
 27. Baláz M, Achimovičová M, Baláz P, Dutková E, Fabián M, Kováčová M, Lukáčová Bujňáková Z, Tóthová E. Mechanochemistry as a versatile and scalable tool for nanomaterials synthesis: recent achievements in Košice, Slovakia. *Curr Opin Green Sust Chem*. 2020;24:7–13.
 28. Lan YC, Minnich AJ, Chen G, Ren ZF. Enhancement of thermoelectric figure-of-merit by a bulk nanostructuring approach. *Adv Funct Mater*. 2010;20:357–76.
 29. He J, Tritt TM. Advances in thermoelectric materials research: Looking back and moving forward. *Science*. 2017;357:eaak9997.
 30. Baláz M, Daneu N, Rajňák M, Kurimský J, Hegedüs M, Dutková E, Fabián M, Kaňuchová M, Baláz P. Rapid mechanochemical synthesis of nanostructured mohite Cu_2SnS_3 (CTS). *J Mater Sci*. 2018;53:13631–42.
 31. Baláz P, Hegedüs M, Reece M, Zhang R, Su T, Škorvánek I, Briančin J, Baláz M, Mihálik M, Tešínský M, Achimovičová M. Mechanochemistry for thermoelectrics: nanobulk $\text{Cu}_6\text{Fe}_2\text{SnS}_8/\text{Cu}_2\text{FeSnS}_4$ composite synthesized in an industrial mill. *J Electron Mater*. 2019;48:1846–56.
 32. Baláz P, Baláz M, Sayagués MJ, Eliyas A, Kostova NG, Kaňuchová M, Dutková E, Zorkovská A. Chalcogenide quaternary $\text{Cu}_2\text{FeSnS}_4$ nanocrystals for solar cells: explosive character of mechanochemical synthesis and environmental challenge. *Crystals*. 2017;7:367.
 33. Baláz P, Baláz M, Zorkovská A, Škorvánek I, Bujňáková Z, Trajic J. Kinetics of solid-state synthesis of quaternary $\text{Cu}_2\text{FeSnS}_4$ (stannite) nanocrystals for solar energy applications. *Acta Phys Pol A*. 2017;131:1153–5.
 34. Baláz P, Baláz M, Sayagués MJ, Škorvánek I, Zorkovská A, Dutková E, Briančin J, Kováč J, Kováč J, Shpotyuk Y. Mechanochemical solvent-free synthesis of quaternary semiconductor Cu–Fe–Sn–S nanocrystals. *Nanoscale Res Lett*. 2017;12:1.
 35. Baláz M, Dobrozhan O, Tešínský M, Zhang R-Z, Džunda R, Dutková E, Rajňák M, Chen K, Reece MJ, Baláz P. Scalable and environmentally friendly mechanochemical synthesis of nanocrystalline rhodostannite ($\text{Cu}_2\text{FeSn}_3\text{S}_8$). *Powder Technol*. 2021;388:192–200.
 36. Baláz P, Hegedüs M, Achimovičová M, Baláz M, Tešínský M, Dutková E, Kaňuchová M, Briančin J. Semi-industrial green mechanochemical syntheses of solar cell absorbers based on quaternary sulfides. *ACS Sust Chem Eng*. 2018;6:2132–41.
 37. Kovalenker VA, Evstigneeva TL, Malov VS, Vyalsov LN. Chatkalite, $\text{Cu}_4\text{FeSn}_2\text{S}_8$, a new mineral. *Mineral Zh*. 1981;3:79–86.
 38. Kovalenker VA. Tin minerals and their parageneses in a near-surface gold deposit. *Geologiya Rudnykh Mestorozhdenij*. 1982;24:31–41.
 39. Marquez-Zavalía MF, Galiski MA. Chatkalita, nekrasovita y otros minerales del grupo de la estannita de veta Maria Eugenia, Cerro Atajo, Catamarca. *Reviasta dee la Asociation Geologica Argentina*. 2007;62:289–98.
 40. Matteazzi P, Le Caër G. Mechanically activated room-temperature reduction of sulfides. *Mater Sci Eng A*. 1992;156:229–37.
 41. Bujňáková Z, Baláz P, Zorkovská A. Enargite concentrate processing by the combination of mechanochemical, hydrometallurgical and precipitation methods. *Int J Miner Process*. 2014;127:28–36.
 42. Dutkova E, Bujnakova Z, Kovac J, Skorvanek I, Sayagues MJ, Zorkovska A, Kovac J, Balaz P. Mechanochemical synthesis,

- structural, magnetic, optical and electrooptical properties of CuFeS₂ nanoparticles. *Adv Powder Technol.* 2018;29:1820–6.
43. Baláž P, Dutková E, Škorvánek I, Gock E, Kováč J, Šatka A. Kinetics of mechanochemical synthesis of Me/FeS (Me=Cu, Pb, Sb) nanoparticles. *J Alloys Compd.* 2009;483:484–7.
 44. J. Rodriguez-Carvajal, Recent development of the program FULL-PROF, in: *Newsletter 26 (2001) 12*, Commission on Powder Diffraction (IUCr), 2001.
 45. National Institute of Standards and Technology (NIST) and Fachinformationszentrum Karlsruhe (FIZ), in: *Inorganic crystal structure database*.
 46. Zak T, Jiraskova Y. CONFIT: Mössbauer spectra fitting program. *Surf Interface Anal.* 2006;38:710–4.
 47. Davis R, John P. Application of Taguchi-based design of experiments for industrial chemical processes. In: Silva V, editor. *Statistical approaches with emphasis on design of experiments applied to chemical processes*. London: IntechOpen; 2015.
 48. Taguchi G, Jugulum R, Taguchi S. *Computer-based robust engineering: essentials for DFSS*. Milwaukee: ASQ Quality Press; 2004.
 49. Zhang FL, Zhu M, Wang CY. Parameters optimization in the planetary ball milling of nanostructured tungsten carbide/cobalt powder. *Int J Refract Metal Hard Mater.* 2008;26:329–33.
 50. Hajji H, Nasr S, Millot N, Ben Salem E. Study of the effect of milling parameters on mechanochemical synthesis of hydroxyfluorapatite using the Taguchi method. *Powder Technol.* 2019;356:566–80.
 51. Mussapyrova L, Nadirov R, Baláž P, Rajňák M, Bureš R, Baláž M. Selective room-temperature leaching of copper from mechanically activated copper smelter slag. *J Mater Res Technol.* 2021;12:2011–25.
 52. Baláž M, Zorkovská A, Urakaev F, Baláž P, Briančin J, Bujňáková Z, Achimovičová M, Gock E. Ultrafast mechanochemical synthesis of copper sulfides. *RSC Adv.* 2016;6:87836–42.
 53. Baláž M, Zorkovská A, Blazquez JS, Daneu N, Baláž P. Mechanochemistry of copper sulphides: phase interchanges during milling. *J Mater Sci.* 2017;52:11947–61.
 54. Scragg JJ, Ericson T, Kubart T, Edoff M, Platzer-Bjorkman C. Chemical insights into instability of Cu₂ZnSnS₄ films during annealing. *Chem Mater.* 2011;23:4625–33.
 55. Yamanaka T, Kato A. Mossbauer-effect study of Fe-57 and Sn-119 in stannite, stannoidite, and mawsonite. *Am Mineral.* 1976;61:260–5.
 56. Suryanarayana C. Mechanical alloying and mixing. *Prog Mater Sci.* 2001;46:1–184.

Publisher's Note Springer Nature remains neutral with regard to jurisdictional claims in published maps and institutional affiliations.